Evidence for High-Efficiency Exciton Dissociation at Polymer/Single-Walled Carbon Nanotube Interfaces in Planar Nano-heterojunction Photovoltaics

Moon-Ho Ham,[†] Geraldine L. C. Paulus,[†] Chang Young Lee,[†] Changsik Song,[†] Kourosh Kalantar-zadeh,[†,‡] Wonjoon Choi,[†] Jae-Hee Han,[†] and Michael S. Strano[†,*]

[†]Department of Chemical Engineering, Massachusetts Institute of Technology, Cambridge, Massachusetts 02139, United States, and [‡]School of Electrical and Computer Engineering, RMIT University, Melbourne, Vic 3001, Australia

ABSTRACT There is significant interest in combining carbon nanotubes with semiconducting polymers for photovoltaic applications because of potential advantages from smaller exciton transport lengths and enhanced charge separation. However, to date, bulk heterojunction (BHJ) devices have demonstrated relatively poor efficiencies, and little is understood about the polymer/nanotube junction. To investigate this interface, we fabricate a planar nano-heterojunction comprising well-isolated millimeter-long single-walled carbon nanotubes underneath a poly(3-hexylthiophene) (P3HT) layer. The resulting junctions display photovoltaic efficiencies per nanotube ranging from 3% to 3.82%, which exceed those of polymer/nanotube BHJs by a factor of 50—100. The increase is attributed to the absence of aggregate formation in this planar device geometry. It is shown that the polymer/nanotube interface itself is responsible for exciton dissociation. Typical open-circuit voltages are near 0.5 V with fill factors of 0.25—0.3, which are largely invariant with the number of nanotubes per device and P3HT thickness. A maximum efficiency is obtained for a 60 nm-thick P3HT layer, which is predicted by a Monte Carlo simulation that takes into account exciton generation, transport, recombination, and dissociation. This platform is promising for further understanding the potential role of polymer/nanotube interfaces for photovoltaic applications.

KEYWORDS: single-walled carbon nanotubes · polymer hybrid solar cells · organic photovoltaics · well-aligned carbon nanotubes · n-doping of carbon nanotubes · Monte Carlo modeling · exciton diffusion

Polymer photovoltaic cells have drawn significant interest as potential alternatives to their inorganic counterparts due to potential economic advantages and efficiencies in large-area fabrication processes.[1−3] Considerable efforts have focused on enhancing the energy conversion efficiency,[3−6] where the best devices constructed to date consist of a mixture of polythiophene derivatives (electron donor) and C_{60} fullerenes (electron acceptor), called a bulk heterojunction (BHJ) type, where the maximum energy conversion efficiency has reached approximately 7% to date.[5−7] In parallel, there have been studies devoted to designing hybrid systems incorporating nanomaterials such as carbon nanotubes,[8−11] inorganic nanowires and nanorods,[12−16] and nanoparticles.[17−19] It is hypothesized that the introduction of carbon nanotubes, in particular, to polymeric semiconductor materials, will improve energy conversion efficiency due to the higher carrier mobility and ballistic conduction pathways provided by the nanotube.[20] To date, however, both multiwalled carbon nanotubes (MWNTs)[8] and single-walled carbon nanotubes (SWNTs)[9−11] BHJ photovoltaic cells have suffered from much lower efficiencies compared to conjugated polymer/fullerene BHJ photovoltaic cells.[5,6] The reasons for this disparity remain an open research question. To address this, in this work we fabricate a highly idealized interface consisting of isolated, electronically contacted chemical vapor deposition (CVD)-grown SWNTs contacting a spin-coated *p*-type poly(3-hexylthiophene) (P3HT) layer. This planar nanoheterojunction device provides a simpler and better defined substrate for exciton dissociation than typical bulk junctions, and is therefore ideal for answering these questions.

It is suspected that some major issues limiting the device performance of carbon nanotube solar cells are bundling/aggregation of nanotubes during polymer dispersion and the coexistence of metallic and semiconducting nanotubes,[21,22] which are key obstacles for exciton dissociation into free carriers. A nanoheterojunction formed by individual SWNTs and polymer can eliminate these variables from the efficiency evaluation. Moreover, P3HT and semiconducting SWNTs were recently presented theoretically and experimentally to form a

*Address correspondence to strano@mit.edu.

Received for review August 6, 2010 and accepted September 24, 2010.

Published online October 1, 2010.
10.1021/nn1019384

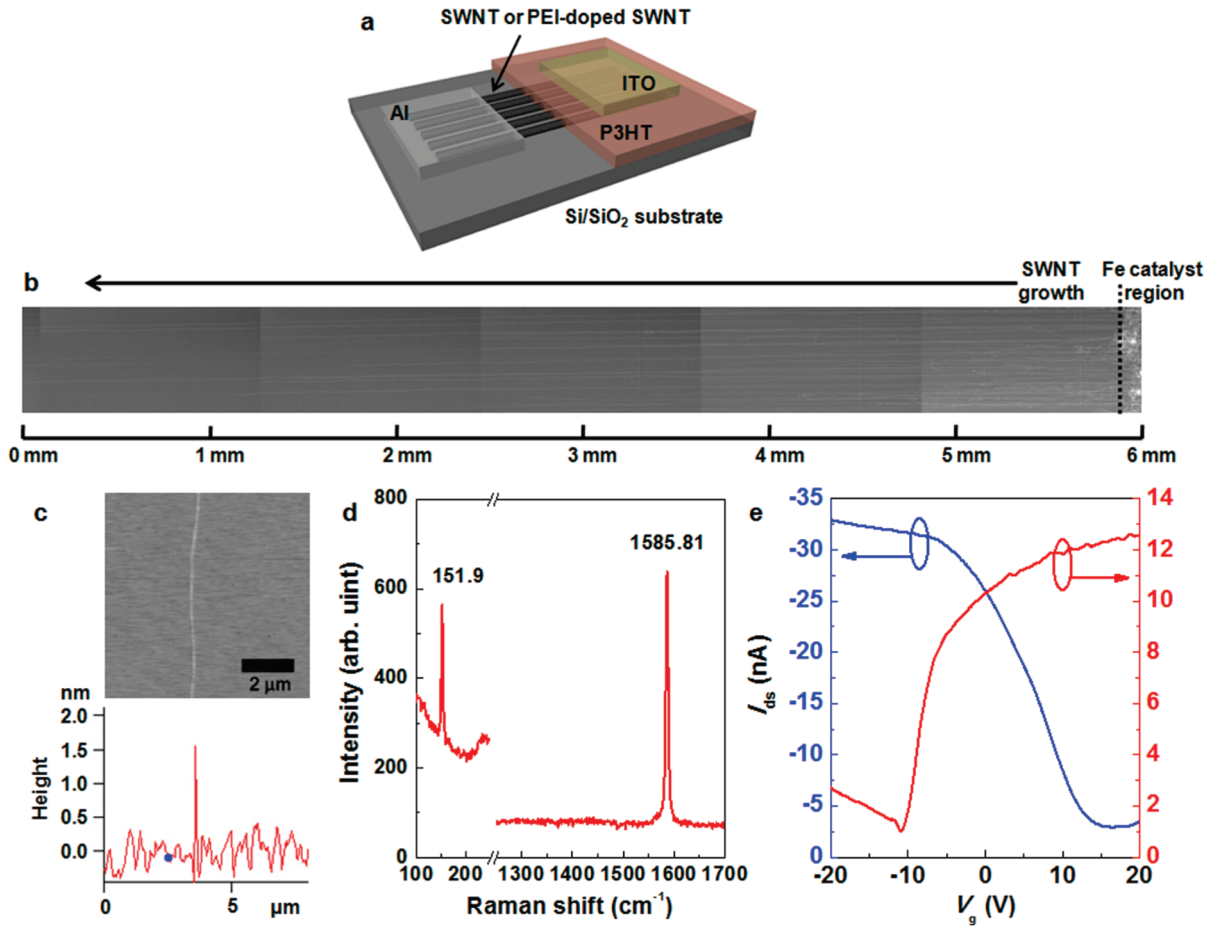

Figure 1. Hybrid planar nanoheterojunction solar cell based on conjugated polymer and carbon nanotubes. (a) Schematic of planar heterojunction solar cell based on a P3HT film on laterally aligned SWNTs. The device has a width of 0.5 mm, a length of 1 mm, and a height of 15−260 nm, depending on the P3HT thickness. (b) A series of SEM images of laterally aligned ultralong SWNT arrays on a Si wafer with a SiO_2 layer, grown by CVD. (c) AFM image (top) and height profile (bottom) of a single SWNT with diameter of ~1.6 nm. (d) Raman spectrum of a typical CVD-grown SWNT utilized in the device, free of a measurable D-peak, obtained using a 633 nm laser for excitation. (e) Transfer curves of SWNT FET before (blue) and after (red) PEI coating on SWNT, demonstrating *p*-type and *n*-type operation, respectively.

type-II heterojunction in P3HT/SWNT nanohybrids,[22,23] which makes the P3HT/SWNT system a promising candidate for organic photovoltaics.

In this work, we report a hybrid planar solar cell based on regioregular P3HT (RR-P3HT) and individually, laterally aligned SWNTs forming a well-defined interface in which the energy conversion efficiency per nanotube reaches 3%. In our system, ultralong, well-aligned SWNTs prepared by CVD serve as direct pathways to an Al electrode for charge collection and rule out unexpected performance deterioration from tube−tube junctions between metallic and semiconducting nanotubes. The highest performing devices are fabricated by polyethylene imine (PEI) coating on the SWNTs in order to convert the SWNTs from *p* to *n* type. The photovoltaic properties of the P3HT/SWNT hybrid nanoheterojunction devices were found to depend on the number of SWNTs and the thickness of P3HT layer with a trend described using a kinetic Monte Carlo (KMC) model of exciton diffusion and reaction.

RESUITS AND DISCUSSION

Figure 1a shows a schematic of the planar nanoheterojunction solar cell based on a P3HT film deposited by spin-coating it onto laterally aligned carbon nanotubes. These SWNTs were grown by CVD and characterized prior to device fabrication. As shown in Figure 1b, the analysis of a series of SEM images recorded along the length of SWNTs reveals perfectly aligned growth of millimeter-long SWNT arrays similar to those produced previously.[24−26] Figure 1c is a representative AFM image of a single SWNT with a diameter of 1.6 nm. The AFM measurements indicate that the SWNTs tested in this work have a diameter distribution of 1.0−2.5 nm. The Raman spectrum in Figure 1d shows obvious radial breathing mode (RBM) and G-mode features. Also, since there is no detectable defect-induced D-mode peak, we conclude that chemical defects, which may also be important centers for exciton dissociation or recombination,[27−31] are largely absent. To directly explore how the Fermi level in the SWNT influences the resulting photovoltaic effect, we converted the SWNT in

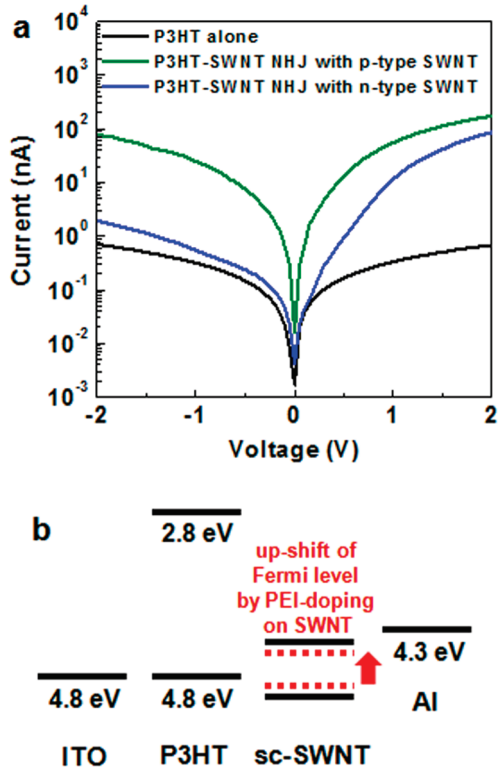

Figure 2. Diode characterizations of P3HT/SWNT nanoheterojuctions. (a) *I*−*V* curves of the devices with P3HT thickness of 60 nm in the dark: P3HT device (black), P3HT/SWNT nanoheterojunction (NHJ) devices with *p*-type SWNTs (green) and *n*-type SWNTs (blue). (b) Schematic energy level diagram of the P3HT/SWNT heterojunction solar cell. For semiconducting SWNTs (sc-SWNTs), the work function, which is defined as the energy difference between the vacuum level and the midgap, and bandgap are 4.73 and ~0.5 eV, respectively.[34−36] The Fermi level of the SWNTs is elevated by PEI doping into the SWNTs, resulting in *n*-type conversion of the SWNTs.

some devices from *p*- to *n*-type using a 20 wt % PEI solution in methanol.[32,33] The arrays were tested as field-effect transistors (FET) with a back-gate geometry to verify the change in the Fermi level. The resulting transfer characteristics in Figure 1e confirm that the arrays were either converted to *n*-type devices after the PEI coating or remained *p*-type without additional coating.

The P3HT/SWNT heterojunction was completed by spin-coating a P3HT layer onto the PEI-coated or uncoated SWNT arrays (Supporting Information, Figure S1). Figure 2a shows the electrical characteristics of the devices with a P3HT thickness of 60 nm in the dark. The P3HT alone shows an almost linear characteristic while the P3HT/SWNT heterojunction devices exhibit behavior that is clearly rectifying. The devices seem to be series resistance limited, but the introduction of SWNTs into the devices makes them less resistive. We estimate that the bandgap of the semiconducting nanotubes is ~0.5 eV from the average diameter of the nanotubes (Supporting Information, Figure S2).[34] Since the work function of the nanotubes is 4.75 eV,[35,36] the P3HT and nanotubes form a type-II heterojunction, as schematically shown in Figure 2b. It has been reported by Kanai *et al.* and Schuettfort *et al.* that a semiconducting nanotube and P3HT form a type II heterojunction, where they presented density functional theory calculations and spectroscopic evidence, respectively.[22,23] For the heterojunction devices, a lower leakage current and a higher on/off ratio were observed for *n*-doped SWNTs. This is interpreted in terms of the formation of better rectifying contacts by elevating the Fermi level of the SWNTs due to *n*-type conversion,[32,33] implying the improved type II band alignment.

The representative current−voltage (*I*−*V*) curves of the devices with either *p*- or *n*-type SWNTs in the dark and under light illumination from a one-sun solar simulator with an AM 1.5G filter are shown in Figure 3a. In both cases, clear photovoltaic behavior was observed upon illumination. The photovoltaic parameters (short-circuit current I_{SC}, open-circuit voltage V_{OC}, and fill factor FF) of the devices with a P3HT thickness of 60 nm are plotted as a function of number of SWNTs, as shown in Figure 3b,c. In the P3HT/SWNT devices, the short-circuit current increases approximately linearly with the number of SWNTs while the open-circuit voltage (V_{OC} = 0.45−0.55 V) and fill factor (FF = 0.25−0.30) remain almost invariant. It is important to note that the presence of carbon nanotubes results in a more than 20-fold increase in the short-circuit current even though the devices have a minimal number of nanotubes. This suggests that the interface created by the carbon nanotubes effectively acts as a dissociation site of the excitons generated by absorption of the photons into free electrons and holes since the introduction of the nanotubes produces the rectifying junction leading to the built-in electric field for exciton dissociation. However due to a minimal number of SWNTs, the series resistance is quite high compared to BHJ solar cells, resulting in a comparatively low fill factor.

Incorporation of *n*-type SWNTs leads to an increase in the open-circuit voltage with a somewhat reduced short-circuit current, as shown in Figure 3a. The increase in the open-circuit voltage is understood by considering the Fermi level change, discussed earlier, whereas the slight decrease in the short-circuit current is most likely due to the introduction of an insulating PEI monolayer (Supporting Information, Figure S2),[32] which limits the carrier transport to some extent (Figure 2b). It is known that the open-circuit voltage is explained either by the metal−insulator−metal (MIM) model or is correlated with the difference between the lowest unoccupied molecular orbital (LUMO) level of the electron acceptor and the highest occupied molecular orbital (HOMO) level of the electron donor although the origin of open-circuit voltage is still a matter of debate.[37] We show that our system has semiconducting nanotubes, as discussed later, of which the open-circuit voltage is not in conjunction with the MIM model. The higher open-circuit voltage after PEI coating in our system can be attributed to up-shifting the Fermi level of the SWNT by adding an electron-

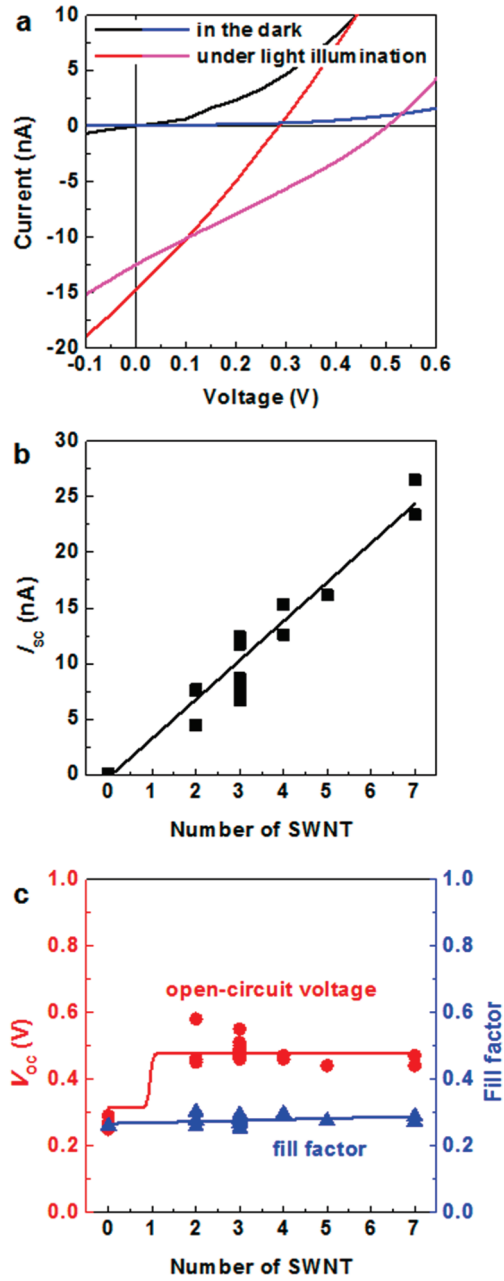

Figure 3. Photovoltaic characterizations of P3HT/SWNT planar nanoheterojunction solar cells with P3HT thickness of 60 nm. (a) *I*−*V* curves of the P3HT/SWNT nanoheterojunction devices with *p*-type SWNTs (black and red) and *n*-type SWNTs (blue and pink) in the dark and under illumination, respectively, from a one-sun solar simulator. (b) Short-circuit current I_{SC} of the P3HT/*n*-SWNT devices as a function of number of SWNTs. (c) Open-circuit voltage V_{OC} and fill factor FF of the P3HT/*n*-SWNT devices as a function of number of SWNTs.

donating functional group, PEI, on the SWNT. Similar tendencies have been found in polymer/fullerene heterojunction solar cells, where the open-circuit voltage was increased by lowering the HOMO level of electron donors.[7,38,39] In particular, Chen *et al.* have attempted to alter the HOMO level of photoactive polymers by adding an electron-withdrawing group, leading to higher V_{OC} and efficiency.[7]

In Figure 3a, a representative *n*-type heterojunction device with 3 SWNTs exhibited an open-circuit voltage (V_{OC}) of 0.5 V, a short-circuit current (I_{SC}) of 12.5 nA and a fill factor (FF) of 0.28. The energy conversion efficiency η per nanotube is estimated as

$$\eta = (I_{SC} \times V_{OC} \times FF)/(P_{in} \times A) \quad (1)$$

where P_{in} is the incident power (P_{in} = 100 mW cm^{-2}) and A is the device area. We note that the true device area is likely the projected exciton capture interface (A),

$$A = W \times L \times N \quad (2)$$

where W is the projected exciton capture distance of one SWNT, L is the length of nanotubes covered by P3HT (L = 1 mm) and N is the number of the SWNT (N = 3). The projected exciton capture distance of the SWNT (W) is estimated as the sum of the SWNT radius (R = ~1 nm) and the exciton diffusion length (L_D = 8.5 nm)[40] on either side of the device (Supporting Information, Figure S5),[41]

$$W = 2(R + L_D) \quad (3)$$

Hence, the energy conversion efficiency per nanotube can be calculated to be 3%. For this device, the nanotubes are about several tens to a few hundred micrometers away from each other. If one packs the device with an optimum spacing between nanotubes, the overall efficiency can reach the maximum of 3.82% (Supporting Information, Figure S5). We note that this estimate is approximately 100 and 50 times higher than those for polymer/SWNT heterojunctions[9,10] and polymer/MWNT[8] solar cells (0.04% and 0.081%), respectively. In order to critically evaluate our results we address two possibilities that our value might be an overestimation of the actual efficiency. When the SWNT suspension and P3HT solution are mixed, the polymer has time to wrap itself around the nanotubes. This may enhance the order of the P3HT chains one-dimensionally along the SWNT surface and increase the effective conjugation length of the polymer due to the formation of highly planar structures of the backbones after the interaction with the SWNT.[11,42,43] However, even this effect is not always observed and seems to happen dominantly in systems developed using solution synthesis methods.[11,42−44] As reported by Chu *et al.*, if a polymer wraps the SWNT by *in situ* polymerization, the effective conjugation length of the composite structure is shorter than that of the pure polymer.[44] Also, Geng *et al.* reported the increased crystallinity of the solid-state P3HT in a P3HT/SWNT composite, but they attributed the effect to the solubilization mechanism of the conjugated polymer on the SWNT.[11] In our devices, the SWNT were not dispersed or mixed in a P3HT solution, but they were attached to the Si/SiO_2 wafer and the spin-coated P3HT on top of the SWNT quickly solidified. As a result, the P3HT has barely any

chance to wrap itself around the SWNT. Therefore, we believe that the increase of the exciton diffusion length due to the enhanced crystallinity is very limited, since due to the fast solidification there is a low possibility of $\pi-\pi$ stacking between P3HT and the SWNT. Secondly, the projected exciton capture distance might be related to the band bending near the nanotubes. Actually, for our modeling which will be discussed later, we used the results reported by Guo *et al*.,[45] where they studied electric-field dependence of polaron yield in RR-P3HT. Band bending occurs in such an electric field (this means the effect of band bending has already been considered in our simulations. On the basis of this, the model does take into account the dissociation of bulk excitons. In addition, the exciton diffusion length has been estimated in the range of 2.6−8.5 nm by using different methods,[40,46−48] and in this work the maximum value of the exciton diffusion length (8.5 nm) was employed. If we were to use the lower limit (2.6 nm),[46] the efficiency would be estimated to be 8% per nanotube. It implies our calculations are valid since 3% per nanotube is a lower estimate of our efficiency based on the exciton diffusion length in P3HT reported so far.

Further, the true device area of the previously reported systems, when compared with our device, is very significant.[8−10] Well-dispersed SWNTs in the bulk of a polymer[8−10] represent an enormous polymer/SWNT interfacial area, much larger than the one in our system. In refs 9 and10 Kymakis *et al*. used a 60 nm-thick P3OT/SWNT BHJ film which contains 1 wt % SWNTs. It follows from a 1 wt % loading of SWNTs

$$0.01 = \frac{m_{SWNT}}{m_{SWNT} + m_{P3OT}} \cong \frac{m_{SWNT}}{m_{P3OT}} \quad (4)$$

where m_{SWNT} and m_{P3OT} are the mass of the SWNTs and P3HT, respectively. The SWNTs used in this case were obtained from Carbolex Inc. with an average of 800 nm in length and 1.4 nm in diameter.[9,10,49] As SWNTs are cylindrical molecules of rolled graphene with carbon atoms on their surface, the comparison of the interface area between polymer/SWNT BHJs and our planar heterojunction as an active site for exciton dissociation is equivalent to comparison of the SWNT mass in the devices. Given by the number of C atoms per nm of SWNTs to be equal to $118.2d_{(n,m)}$ (where $d_{(n,m)}$ is the diameter in nm), the weight of one SWNT in the BHJ is calculated by

$$m_{1SWNT} = (\text{the number of C atoms per nm SWNT}) \times (\text{average length}) \times (\text{weight of one C}) \quad (5)$$

which results in $m_{1SWNT} \approx 2.55 \times 10^{-18}$ g. Since the thickness of the P3OT layer is 60 nm and the density of P3OT is 1.05 g/cm^3,[50] the mass of P3OT per cm^2 surface area is 6.3×10^{-6} g/cm^2. From equation (4) we then deduce $m_{SWNT} \approx 6.3 \times 10^{-8}$ g/cm^2. Dividing the mass of all the SWNTs by the mass of one SWNT gives the number of SWNTs present in the system investigated by Kymakis *et al*. as 2.47×10^{10} SWNTs per cm^2 surface area. Considering that the device area is the same as our device area (500 μm × 1 mm), the BHJ device with 1 wt % SWNTs has 1.24×10^8 SWNTs. Comparatively, our planar systems comprise 1−10 nanotubes. Taking the upper limit of 10 nanotubes, which have a length of 1 mm, this means 1250 800 nm-long SWNTs, approximately 5 orders of magnitude smaller compared to the value for the work carried out by Kymakis *et al*. We calculate the actual device area for Kymakis' system by the same standard used for our own system, considering the diffusion length of excitons (L_D') in P3OT equals ∼5 nm.[51] The actual device area (A') is estimated as

$$A' = W' \times L' \times N' \quad (6)$$

where W' is the projected exciton capture distance of one SWNT ($W' = 2(R' + L_D')$), L' is the length of the SWNT ($L' = 800$ nm), and N' is the number of SWNTs ($N' = 1.24 \times 10^8$). Their actual device area is calculated to be 2.25 cm^2 per cm^2 surface area, whereas in our system the area comes out to be 0.00038 cm^2 per cm^2 surface area, which is ∼5900 times smaller than our case. Although the actual efficiency of the heterojunction device, which is calculated by considering whole device area, is fairly low ($\sim 3.5 \times 10^{-4}$%) because of the small number of SWNTs in the device, comparison of the surface area of our devices with a polymer/SWNT BHJ device reported by Kymakis *et al*.[9,10] supports that the efficiency per nanotube in our devices is much higher. It is also noteworthy that efficiency in this work is actually comparable to those for polymer/fullerene BHJ solar cells (3−6%).[5,6]

The most obvious reason for the increase in efficiency over BHJ devices based on the polymer/SWNT system is that the carbon nanotube interface in this work is free from bundled aggregates compared to the interface of the polymer/carbon nanotube solar cells reported in literature[8−11] where fabrication proceeded from a colloidal dispersion of nanotubes. Raman spectroscopy provides an additional insight into the workings of the planar device. We find that approximately 90% of semiconducting SWNTs typically comprise the device (Figure 4a−c).[52] More importantly, as the nanotubes were grown in parallel, there are no tube−tube junctions between metallic and semiconducting SWNTs. These junctions may be sources of exciton recombination sites in bundled aggregates.[21,22] Having semiconducting SWNTs without the interruption of metallic SWNTs could give rise to a strong built-in electric field at the interface between semiconducting SWNTs and the P3HT layer[22,23] where the separated charges are directly transported to the electrode through the nanotubes with little or no loss. We also note that the high quality of the SWNTs grown by CVD leads to higher efficiency since the D-mode peak was not observed (Fig-

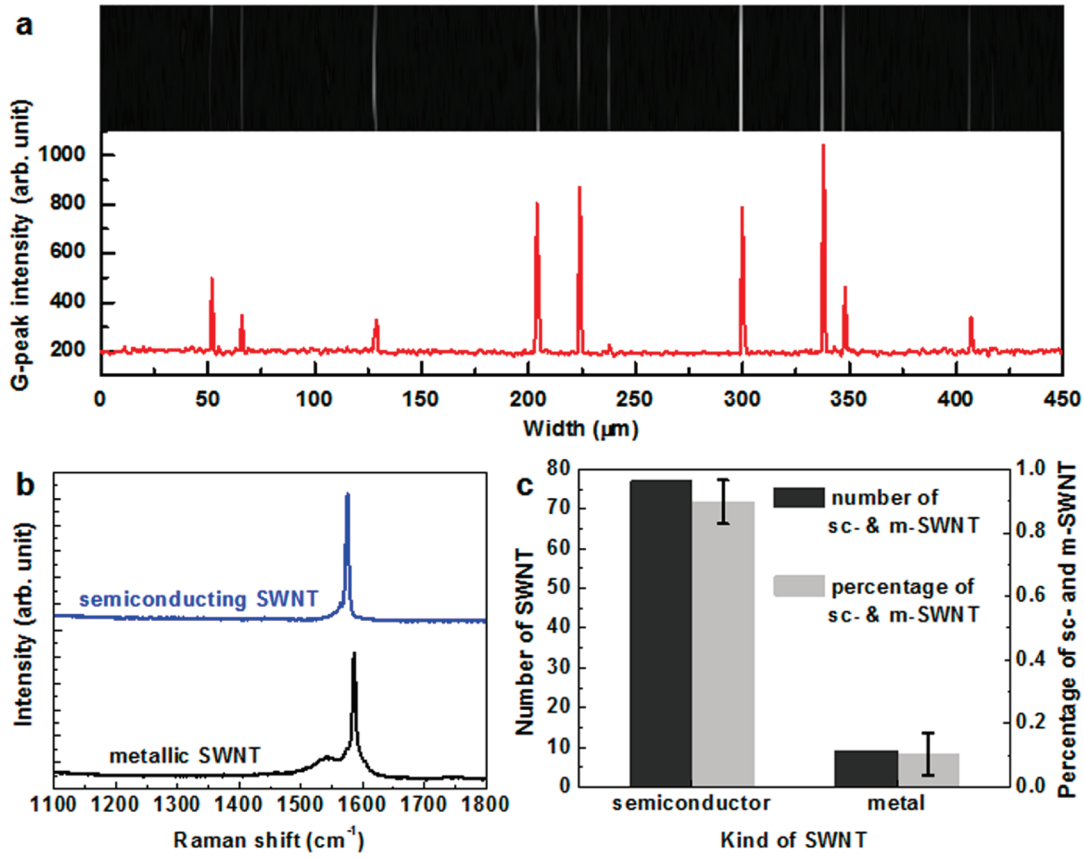

Figure 4. Raman spectroscopy of laterally aligned SWNTs grown by CVD. (a) Raman mapping image (top) produced by integrating G-mode region around 1590 cm^{-1} and G-peak intensities (bottom) of SWNTs, obtained using a 633 nm laser for excitation. (b) Representative Raman spectra of semiconducting and metallic SWNTs.[52] (c) The number of semiconducting (sc-) and metallic (m-) SWNTs, and the percentage of sc- and m-SWNTs, obtained from Raman spectra. The Raman results indicate that our CVD-grown nanotubes contain nearly 90% of the semiconductors.

ures 1d and 4b). The implication is that high-efficiency photovoltaic devices involving SWNTs should use purified semiconducting nanotubes, preferably of low defect density and in an unbundled state (well-dispersed) to realize photovoltaic performances comparable or superior to that of BHJ solar cells. An additional advantage of our planar nano-heterojunction is that once charges dissociate (most of them at the interface between P3HT and SWNT[45]), they reach their respective electrodes more easily and faster compared to free charge carriers generated in BHJ solar cells.

Figure 5 shows the energy conversion efficiency per nanotube as a function of P3HT thickness. The open-circuit voltage (~0.46 V) and the fill factor (~0.28) are fairly constant for varying P3HT thicknesses, but like the efficiency, the short-circuit current shows a maximum at 60 nm. Although a similar result has been reported for planar P3HT and [6,6]-phenyl-C_{61}-butyric acid methyl ester (PCBM) solar cells,[53] the reason for the maximum short-circuit current at a polymer thickness of 60 nm is less evident. One would expect the maximum photocurrent output is obtained when the P3HT thickness is either near 8.5 nm, which is the value of the diffusion length of singlet excitons in pristine RR-P3HT[40] or about 300 nm to absorb most light. In our device, the structure is planar and the SWNTs are well-aligned in parallel. As the main dissociation site is the interface

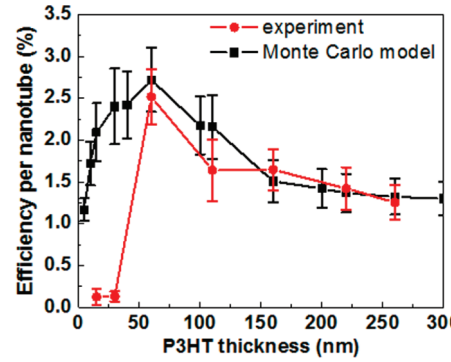

Figure 5. Energy conversion efficiency per nanotube of the devices as a function of P3HT thickness. The red circles are the experimental results from the devices with P3HT thicknesses ranging from 15 to 260 nm, and the black squares are the results calculated from the KMC model. The experimental efficiencies are calculated with a real projected device area, $A = 2(L_D + R) \times N \times L$, and the theoretical efficiencies are predicted with $V_{OC} = 0.46$ V and FF = 0.28. A maximum efficiency is found for a P3HT thickness of 60 nm with a good agreement between experiment and model. Error bars for the experimental data indicate one standard deviation for 4−15 devices. For the KMC model, the error bars indicate the standard deviation of 400 successive simulation runs at each thickness.

between the SWNTs and the polymer and the absorption of light shows a quasi-exponential decrease with depth in the polymer (Supporting Information, Figure S7), the presumption of 300 nm which is beneficial only for BHJ solar cells can be excluded,[54] but the value of the diffusion length of singlet excitons is used in the following simulation.

We developed a KMC model in order to understand short-circuit current as a function of P3HT thickness. The results are shown in Figure 5 together with the experimental data. The details of this model are described in Supporting Information section 5. It is based on a 3.9 nm × 1.61 nm × 0.39 nm lattice structure for RR-P3HT (Supporting Information, Figure S6) and takes into account the spatial and energetic disorder of the polymer. The model focuses on tracking the diffusion and dissociation of excitons throughout this lattice, given the fact that they dominate the efficiency in the device.[55] The exciton generation throughout the lattice is modeled following Beer's law, taking into account the possible interference effects (Supporting Information, Figure S7). In this planar nanoheterojunction device, exciton diffusion is modeled using a Miller−Abrahams expression,[56,57] as opposed to the case of the BHJ devices, where exciton hopping is dominated by Förster resonance energy transfer (FRET).[55,58−60] Excitons can diffuse throughout the lattice, recombine radiatively, nonradiatively (by "hopping" into a "trap" which represents a defect in the polymer), or dissociate. The top layer of the lattice is assumed to have a much higher percentage of traps (75% *vs* 10% in the bulk) since sputtering of the ITO on top of the polymer is known to provide additional quenching sites for the excitons (Supporting Information, Figures S3 and S4).[58,61] To predict the maximum in the efficiency at a P3HT thickness of 60 nm, there must be a thickness-dependent exciton sink. Although more research in this area is required, one possible explanation lies in the recent theoretical prediction[45] and experimental observations[53,62] that the electric field created by the heterojunction is strong enough to dissociate a fraction of the generated excitons into free polarons in the bulk as well, as opposed to only at the interface. Since the resultant free electrons have a high chance of recombining with a hole in the bulk of the *p*-doped P3HT,[63] we assume they do not contribute to the current output, which implies a loss in device efficiency. This effect is more pronounced for devices with thinner polymer layers (Supporting Information, section 5). A combination of the exciton generation pattern throughout the polymer slab, a higher trap density in the top layer of the P3HT, and the partial dissociation of excitons in the bulk of the polymer results in a maximum short-circuit current (and thus efficiency) at a polymer thickness of 60 nm (Figure 5). Thus, the experimental observation is consistent with the theoretical prediction based on the KMC model. Another possibility is a higher sputtering damage (that extends deeper into the P3HT). Although an additional study is required to address nontrivial discrepancies at a very low P3HT thickness, the fidelity between the experiment and the results of this simplified KMC model may lead to further insights into photoconversion mechanisms and optimization and ultimately inform BHJ analogues to the planar device we have created in this work.

CONCLUSIONS

We conclude that the primary reasons for low energy conversion efficiency in BHJ devices incorporating SWNTs are (1) the formation of bundled aggregates as a consequence of incomplete polymer dispersion and (2) the presence of tube−tube junctions created for the same reason. The primary evidence for this is that the planar heterojunction device introduced in this work includes neither of these complications and results in a dramatically higher efficiency per nanotube of approximately 3%. The planar nanoheterojunction devices, comprising well-isolated millimeter-long SWNTs underneath a P3HT layer, display efficiencies per nanotube that exceed those of polymer/nanotube BHJs by a factor of 50−100. It is clear from our results that the polymer/nanotube interface itself is responsible for exciton dissociation. Typical open-circuit voltages are near 0.5 V with fill factors of 0.25−0.3, which are largely invariant with the number of nanotubes per device and P3HT thickness. The maximum efficiency observed for 60 nm-thick P3HT layer is predicted by a KMC simulation that takes into account exciton generation, transport, recombination, and dissociation, including a thickness dependent exciton sink that is shown to be important for capturing this effect. It is suggested that this device structure provides a suitable platform for further understanding the potential role of polymer/nanotube interfaces for photovoltaic applications.

EXPERIMENTAL METHODS

SWNTs were laterally grown with lengths greater than 5 mm on the surface of a Si substrate by CVD under steady and stable laminar gas flow from a mixture of ultrahigh-purity (99.999%) methane (CH_4) and hydrogen (H_2).[24−26] A Si substrate with a thermally grown 500 nm-thick SiO_2 layer, coated with a patterned, 5 Å-thick Fe strip as a seed layer, was annealed at 550 °C in air to create Fe oxide islands. The temperature was subsequently raised to 950 °C at a rate of 20 °C/min and maintained for 30 min with a flow of hydrogen, followed by the growth of the SWNTs at 980−1020 °C for 3 h 30 min by adding a flow of methane. After growth, the SWNTs employed to create the heterojunction were characterized by scanning electron microscopy (SEM), atomic force microscopy (AFM), and Raman spectroscopy before application of the P3HT layer.

For the electrical conversion of the SWNTs from *p*-type to *n*-type in some of the devices, a 20 wt % PEI solution in methanol was drop-cast on the SWNT sample, followed by rinsing with

methanol. The resulting PEI layer was essentially a monolayer or submonolayer, with negligible height variations detected by AFM (Supporting Information, Figure S2).[32] A SWNT field-effect transistor (FET) was fabricated with the back-gate geometry, and its electrical properties were examined with an Agilent E5270B semiconductor parameter analyzer (SPA).

The P3HT/SWNT heterojunction solar cells were fabricated using RR-P3HT dissolved in chloroform at concentrations ranging from 1 to 25 mg/mL and spin-coating this mixture onto the PEI-coated or uncoated SWNT arrays, such that approximately a fifth of the array was covered by a 0.5 mm $\times$1 mm P3HT layer (Figure 1a, and Supporting Information, Figure S1). The portion of the SWNT array that is not coated by P3HT was then contacted with Al, which was deposited with the thickness of 60 nm using an e-beam evaporator to form the cathode. A 60 nm-thick ITO patterned layer was subsequently deposited on the P3HT section by sputtering to form the anode. The devices were annealed at 170 °C for 1 min. As a control, a device with only P3HT and no SWNTs was fabricated by spin-coating P3HT solution, and Al and ITO electrodes were subsequently deposited on the P3HT layer.

The photovoltaic properties of the P3HT/SWNT heterojunction devices were characterized by applying the voltage to the ITO electrode with the SPA under illumination from a standard solar simulator (Oriel Instrument, model 91195, 100 mW/cm^2) with an AM 1.5G filter which was calibrated with a reference Si cell certified by the National Renewable Energy Laboratory (NREL).

Acknowledgment. This work was financially supported by a grant from ENI Petroleum Co. Inc. Eni SpA under the Eni-MIT Alliance Solar Frontiers Program. M.H.H. is grateful for support from the Korea Research Foundation Grant funded by the Korean Government (MOEHRD) (KRF-2007-357-D00133).

Supporting Information Available: (1) Schematic of overall process for the P3HT/SWNT planar photovoltaic device fabrication, (2) AFM results of SWNT before and after PEI coating on the SWNTs, (3) Characterizations of P3HT films before and after ITO deposition by sputtering, (4) energy conversion efficiency calculation, and (5) background and details of the kinetic Monte Carlo model. This material is available free of charge *via* the Internet at http://pubs.acs.org.

REFERENCES AND NOTES

1. Tang, C. W. Two-Layer Organic Photovoltaic Cell. *Appl. Phys. Lett.* **1986**, *48*, 183–185.
2. Sariciftci, N. S.; Smilowitz, L.; Heeger, A. J.; Wudl, F. Photoinduced Electron Transfer from a Conducting Polymer to Buckminsterfullerene. *Science* **1992**, *258*, 1474–1476.
3. Gunes, S.; Neugebauer, H.; Sariciftci, N. S. Conjugated Polymer-Based Organic Solar Cells. *Chem. Rev.* **2007**, *107*, 1324–1338.
4. Halls, J. J. M.; Walsh, C. A.; Greenham, N. C.; Marseglia, E. A.; Friend, R. H.; Moratti, S. C.; Holmes, A. B. Efficient Photodiodes from Interpenetrating Polymer Networks. *Nature* **1995**, *376*, 498–500.
5. Li, G.; Shrotriya, V.; Huang, J.; Yao, Y.; Moriarty, T.; Emery, K.; Yang, Y. High-Efficiency Solution Processable Polymer Photovoltaic Cells by Self-Organization of Polymer Blends. *Nat. Mater.* **2005**, *4*, 864–868.
6. Kim, J. Y.; Lee, K.; Coates, N. E.; Moses, D.; Nguyen, T. Q.; Dante, M.; Heeger, A. J. Efficient Tandem Polymer Solar Cells Fabricated by All-Solution Processing. *Science* **2007**, *317*, 222–225.
7. Chen, H. Y.; Hou, J.; Zhang, S.; Liang, Y.; Yang, G.; Yang, Y.; Yu, L.; Wu, Y.; Li, G. Polymer Solar Cells with Enhanced Open-Circuit Voltage and Efficiency. *Nat. Photonics* **2009**, *3*, 649–653.
8. Ago, H.; Petritsch, K.; Shaffer, M. S. P.; Windle, A. H.; Friend, R. H. Composites of Carbon Nanotubes and Conjugated Polymers for Photovoltaic Devices. *Adv. Mater.* **1999**, *11*, 1281–1285.
9. Kymakis, E.; Amaratunga, G. A. J. Single-Wall Carbon Nanotube/Conjugated Polymer Photovoltaic Devices. *Appl. Phys. Lett.* **2002**, *80*, 112–114.
10. Kymakis, E.; Koudoumas, E.; Franghiadakis, I.; Amaratunga, G. A. J. Post-Fabrication Annealing Effects in Polymer-Nanotube Photovoltaic Cells. *J. Phys. D: Appl. Phys.* **2006**, *39*, 1058–1062.
11. Geng, J.; Zeng, T. Influence of Single-Walled Carbon Nanotubes Induced Crystallinity Enhancement and Morphology Change on Polymer Photovoltaic Devices. *J. Am. Chem. Soc.* **2006**, *128*, 16827–16833.
12. Huynh, W. U.; Dittmer, J. J.; Alivisatos, A. P. Hybrid Nanorod−Polymer Solar Cells. *Science* **2002**, *295*, 2425–2427.
13. Novotny, C. J.; Yu, E. T.; Yu, P. K. L. InP Nanowire/Polymer Hybrid Photodiode. *Nano Lett.* **2008**, *8*, 775–779.
14. Briseno, A. L.; Holcombe, T. W.; Boukai, A. I.; Garnett, E. C.; Shelton, S. W.; Frechet, J. J. M.; Yang, P. Oligo- and Poly-thiophene/ZnO Hybrid Nanowire Solar Cells. *Nano Lett.* **2010**, *10*, 334–340.
15. Greene, L. E.; Law, M.; Yuhas, B. D.; Yang, P. ZnO−TiO_2 Core−Shell Nanorod/P3HT Solar Cells. *J. Phys. Chem. C* **2007**, *111*, 18451–18456.
16. Huang, J. S.; Hsiao, C. Y.; Syu, S. J.; Chao, J. J.; Lin, C. F. Well-Aligned Single-Crystalline Silicon Nanowire Hybrid Solar Cells on Glass. *Sol. Energy Mater. Sol. Cells* **2009**, *93*, 621–624.
17. Beek, W. J. E.; Wienk, M. M.; Janssen, R. A. J. Efficient Hybrid Solar Cells from Zinc Oxide Nanoparticles and a Conjugated Polymer. *Adv. Mater.* **2004**, *16*, 1009–1013.
18. Cui, D.; Xu, J.; Zhu, T.; Paradee, G.; Ashok, S.; Gerhold, M. Harvest of Near Infrared Light in PbSe Nanocrystal−Polymer Hybrid Photovoltaic Cells. *Appl. Phys. Lett.* **2006**, *88*, 183111.
19. Chen, H. Y.; Lo, M. K. F.; Yang, G.; Monbouquette, H. G.; Yang, Y. Nanoparticle-Assisted High Photoconductive Gain in Composites of Polymer and Fullerene. *Nat. Nanotechnol.* **2008**, *3*, 543–547.
20. Reich, S.; Thomsen, C.; Maultzsch, J. *Carbon Nanotubes*; Wiley: New York, 2004.
21. Liu, L.; Stanchina, W. E.; Li, G. Effects of Semiconducting and Metallic Single-Walled Carbon Nanotubes on Performance of Bulk Heterojunction Organic Solar Cells. *Appl. Phys. Lett.* **2009**, *94*, 233309.
22. Kanai, Y.; Grossman, J. C. Role of Semiconducting and Metallic Tubes in P3HT/Carbon-Nanotube Photovoltaic Heterojunctions: Density Functional Theory Calculations. *Nano Lett.* **2008**, *8*, 908–912.
23. Schuettfort, T.; Nish, A.; Nicholas, R. J. Observation of a Type II Heterojunction in a Highly Ordered Polymer−Carbon Nanotube Nanohybrid Structure. *Nano Lett.* **2009**, *9*, 3871–3876.
24. Zheng, L. X.; O'Connell, M. J.; Doorn, S. K.; Liao, X. Z.; Zhao, Y. H.; Akhadov, E. A.; Hoffbauer, M. A.; Roop, B. J.; Jia, Q. X.; Dye, R. C.; *et al.* Ultralong Single-Wall Carbon Nanotubes. *Nat. Mater.* **2004**, *3*, 673–676.
25. Jin, Z.; Chu, H.; Wang, J.; Hong, J.; Tan, W.; Li, Y. Ultralow Feeding Gas Flow Guiding Growth of Large-Scale Horizontally Aligned Single-Walled Carbon Nanotube Arrays. *Nano Lett.* **2007**, *7*, 2073–2079.
26. Kang, S. J.; Kocabas, C.; Ozel, T.; Shim, M.; Pimparkar, N.; Alam, M. A.; Rotkin, S. V.; Rogers, J. A. High-Performance Electronics Using Dense, Perfectly Aligned Arrays of Single-Walled Carbon Nanotubes. *Nat. Nanotechnol.* **2007**, *2*, 230–236.
27. Riggs, J. E.; Guo, Z.; Carroll, D. L.; Sun, Y. P. Strong Luminescence of Solubilized Carbon Nanotubes. *J. Am. Chem. Soc.* **2000**, *122*, 5879–5880.
28. Sun, Y. P.; Zhou, B.; Henbest, K.; Fu, K.; Huang, W.; Lin, Y.; Taylor, S.; Carroll, D. L. Luminescence Anisotropy of Functionalized Carbon Nanotubes in Solution. *Chem. Phys. Lett.* **2002**, *351*, 349–353.
29. Banerjee, S.; Wong, S. S. Structural Characterization, Optical Properties, and Improved Solubility of Carbon

Nanotubes Functionalized with Wilkinson's Catalyst. *J. Am. Chem. Soc.* **2002**, *124*, 8940–8948.
30. Lin, Y.; Zhou, B.; Martin, R. B.; Henbest, K. B.; Harruff, B. A.; Riggs, J. E.; Guo, Z. X.; Allard, L. F.; Sun, Y. P. Visible Luminescence of Carbon Nanotubes and Dependence on Functionalization. *J. Phys. Chem. B* **2005**, *109*, 14779–14782.
31. Zhou, B.; Lin, Y.; Veca, L. M.; Fernando, K. A. S.; Harruff, B. A.; Sun, Y. P. Luminescence Polarization Spectroscopy Study of Functionalized Carbon Nanotubes in a Polymeric Matrix. *J. Phys. Chem. B* **2006**, *110*, 3001–3006.
32. Shim, M.; Javey, A.; Kam, N. W. S.; Dai, H. Polymer Functionalization for Air-Stable N-Type Carbon Nanotube Field-Effect Transistors. *J. Am. Chem. Soc.* **2001**, *123*, 11512–11513.
33. Li, Z.; Saini, V.; Dervishi, E.; Kunets, V. P.; Zhang, J.; Xu, Y.; Biris, A. R.; Salamo, G. J.; Biris, A. S. Polymer Functionalized N-Type Single Wall Carbon Nanotube Photovoltaic Devices. *Appl. Phys. Lett.* **2010**, *96*, 033110.
34. Wildoer, J. W. G.; Venema, L. C.; Rinzler, A. G.; Smalley, R. E.; Dekker, C. Electronic Structure of Atomically Resolved Carbon Nanotubes. *Nature* **1998**, *391*, 59–62.
35. Zhao, J.; Han, J.; Lu, J. P. Work Functions of Pristine and Alkali-Metal Intercalated Carbon Nanotubes and Bundles. *Phys. Rev. B* **2002**, *65*, 193401.
36. Suzuki, S.; Watanabe, Y.; Homma, Y.; Fukuba, S. Y.; Heun, S.; Locatelli, A. Work Functions of Individual Single-Walled Carbon Nanotubes. *Appl. Phys. Lett.* **2004**, *85*, 127–129.
37. Brabec, C. J.; Cravino, A.; Meissner, D.; Sariciftci, N. S.; Fromherz, T.; Rispens, M. T.; Sanchez, L.; Hummelen, J. C. Origin of the Open Circuit Voltage of Plastic Solar Cells. *Adv. Funct. Mater.* **2001**, *11*, 374–380.
38. Wang, E.; Wang, L.; Lan, L.; Luo, C.; Zhuang, W.; Peng, J.; Cao, Y. High-Performance Polymer Heterojunction Solar Cells of a Polysilafluorene Derivative. *Appl. Phys. Lett.* **2008**, *92*, 033307.
39. Mutolo, K. L.; Mayo, E. I.; Rand, B. P.; Forrest, S. R.; Thompson, M. E. Enhanced Open-Circuit Voltage in Subphthalocyanine/C_{60} Organic Photovoltaic Cells. *J. Am. Chem. Soc.* **2006**, *128*, 8108–8109.
40. Shaw, P. E.; Ruseckas, A.; Samuel, I. D. W. Exciton Diffusion Measurements in Poly(3-hexylthiophene). *Adv. Mater.* **2008**, *20*, 3516–3520.
41. This 3% value is a lower bound on the efficiency, since the effective device area cannot reasonably exceed the exciton diffusion length, L_D. If instead the physical device area is utilized ($W = 2R$), an unrealistic efficiency of 28.8% is predicted.
42. Ikeda, A.; Nobusawa, K.; Hamano, T; Kikuchi, J. Single-Walled Carbon Nanotubes Template the One-Dimensional Ordering of a Polythiophene Derivative. *Org. Lett.* **2006**, *8*, 5489–5492.
43. Schuettfort, T.; Snaith, H. J.; Nish, A.; Nicholas, R. J. Synthesis and Spectroscopic Characterization of Solution Processable Highly Ordered Polythiophene−Carbon Nanotube Nanohybrid Structures. *Nanotechnology* **2010**, *21*, 025201.
44. Chu, S.; Yi, W.; Wang, S.; Li, F.; Feng, W.; Gong, Q. Steady-State and Transient-State Optical Properties of a Charge-Transfer Composite Material MO-PPV/SWNTs. *Chem. Phys. Lett.* **2008**, *451*, 116–120.
45. Guo, J.; Ohkita, H.; Benten, H.; Ito, S. Near-IR Femtosecond Transient Absorption Spectroscopy of Ultrafast Polaron and Triplet Exciton Formation in Polythiophene Films with Different Regioregularities. *J. Am. Chem. Soc.* **2009**, *131*, 16869–16880.
46. Kroeze, J. E.; Savenije, T. J.; Vermeulen, M. J. W.; Warman, J. M. Contactless Determination of the Photoconductivity Action Spectrum, Exciton Diffusion Length, and Charge Separation Efficiency in Polythiophene-Sensitized TiO_2 Bilayers. *J. Phys. Chem. B* **2003**, *107*, 7696–7705.
47. Lüer, L.; Egelhaaf, H. J.; Oelkrug, D.; Cerullo, G.; Lanzani, G.; Huisman, B. H.; de Leeuw, D. Oxygen-Induced Quenching of Photoexcited States in Polythiophene Films. *Org. Electron.* **2004**, *5*, 83–89.
48. Goh, C.; Scully, S. R.; McGehee, M. D. Effects of Molecular Interface Modification in Hybrid Organic−Inorganic Photovoltaic Cells. *J. Appl. Phys.* **2007**, *101*, 114503.
49. Zhang, Q.; Vichchulada, P.; Cauble, M. A.; Lay, M. D. Percolation in Networks of Aligned SWNTs Formed with Laminar Flow Deposition. *J. Mater. Sci.* **2009**, *44*, 1206–1211.
50. Moulton, J.; Smith, P. Gel Processing of Electrically Conductive Blends of Poly(3-octylthiophene) and Ultrahigh Molecular Weight Polyethylene. *J. Polym. Sci., Part B* **1992**, *30*, 871–878.
51. van der Zanden, B.; van de Krol, R.; Schoonman, J.; Goossens, A. Enhanced Photoluminescence at Poly(3-octyl-thiophene)/TiO_2 Interfaces. *Appl. Phys. Lett.* **2004**, *84*, 2539–2541.
52. Dresselhaus, M. S.; Dresselhaus, G.; Saito, R.; Jorio, A. Raman Spectroscopy of Carbon Nanotubes. *Phys. Rep. Rev.* **2005**, *409*, 47–99.
53. Kim, B. J.; Miyamoto, Y.; Ma, B.; Frechet, J. M. J. Photocrosslinkable Polythiophenes for Efficient, Thermally Stable, Organic Photovoltaics. *Adv. Funct. Mater.* **2009**, *19*, 2273–2281.
54. Peumans, P.; Yakimov, A.; Forrest, S. R. Small Molecular Weight Organic Thin-Film Photodetectors and Solar Cells. *J. Appl. Phys.* **2003**, *93*, 3693–3723.
55. Yang, F.; Forrest, S. R. Photocurrent Generation in Nanostructured Organic Solar Cells. *ACS Nano* **2008**, *2*, 1022–1032.
56. Miller, A.; Abrahams, E. Impurity Conduction at Low Concentrations. *Phys. Rev.* **1960**, *120*, 745–755.
57. Scheidler, M.; Lemmer, U.; Kersting, R.; Karg, S.; Riess, W.; Cleve, B.; Mahrt, R. F.; Kurz, H.; Bässler, H.; Göbel, E. O.; *et al. Monte Carlo Study of Picosecond Exciton Relaxation and Dissociation in Poly(phenylenevinylene). Phys. Rev. B* **1996**, *54*, 5536–5544.
58. Gu, G.; Bulovic, V.; Burrows, P. E.; Forrest, S. R.; Thompson, M. E. Transparent Organic Light Emitting Devices. *Appl. Phys. Lett.* **1996**, *68*, 2606–2608.
59. Watkins, P. K.; Walker, A. B.; Verschoor, G. L. B. Dynamical Monte Carlo Modelling of Organic Solar Cells: The Dependence of Internal Quantum Efficiency on Morphology. *Nano Lett.* **2005**, *5*, 1814–1818.
60. Nelson, J. Diffusion-Limited Recombination in Polymer-Fullerene Blends and Its Influence on Photocurrent Collection. *Phys. Rev. B* **2003**, *67*, 155209.
61. Ahlswede, E.; Hanisch, J.; Powalla, M. Influence of Cathode Sputter Deposition on Organic Solar Cells. *Appl. Phy. Lett.* **2007**, *90*, 063513.
62. Gowrishankar, V.; Scully, S. R.; McGehee, M. D.; Wang, Q.; Branz, H. M. Exciton Splitting and Carrier Transport across the Amorphous-Silicon/Polymer Solar Cell Interface. *Appl. Phys. Lett.* **2006**, *89*, 252102.
63. Yang, K.; Wang, Y.; Jain, A.; Samulson, L.; Kumar, J. Determination of Electron and Hole Mobility of Regioregular Poly(3-hexylthiophene) by the Time of Flight Method. *J. Macromol. Sci., Part A* **2007**, *44*, 1261–1264.